THE PENNSYLVANIA STATE UNIVERSITY
SCHREYER HONORS COLLEGE

DEPARTMENT OF PHYSICS

OPTIMIZING THE POWER OUTPUT OF LUMINESCENT SOLAR CONCENTRATORS THAT USE WHITE DIFFUSIVE BACKGROUNDS

JONATHON R. SCHRECENGOST
SPRING 2018

A thesis
submitted in partial fulfillment
of the requirements
for a baccalaureate degree
in Physics
with honors in Physics

Reviewed and approved* by the following:

Bruce P. Wittmershaus
Associate Professor of Physics
Thesis Supervisor

Darren Williams
Professor of Astronomy and Astrophysics, Physics
Honors Adviser

* Signatures are on file in the Schreyer Honors College.

ABSTRACT

Luminescent solar concentrators (LSCs) have the potential of converting solar energy into electricity less expensively than a standard photovoltaic (PV) panel. LSCs are thin plates of plastic or glass that contain fluorescent material throughout the plate or in a thin film adhered to the surface. The fluorescent material absorbs sunlight and its fluorescence is concentrated onto PV cells along the edges of an LSC using total internal reflection. Some light is able to pass through the LSC and does not reach the PV cells. A white diffusive scattering surface, or white background, is able to scatter this light back into the LSC for another chance of reaching the PV cells. The results of my experimental and theoretical research reveal that using white backgrounds larger than the area of the LSC can further increase its power output. Larger backgrounds produce more power, but with diminishing returns. An optimal air gap between the LSC and a larger white background is required to achieve maximum benefit. The size of this optimal air gap increases as the area of the white background increases. The predictions of my theoretical model agree with my experimental results for the relative performance of these larger white backgrounds with respect to their size and separation from the LSC. Experimental results show an optimal air gap of 10.7 cm separating an LSC from a white background with an area 16 times larger than the LSC. In this configuration, the LSC produced 28% more power than the maximum power output of the LSC using a white background of the same area, and 54% more power than the LSC with no white background present.

TABLE OF CONTENTS

LIST OF FIGURES

ACKNOWLEDGEMENTS

I was able to make a lot of progress in my three years of research at Penn State Behrend, but I would not have made any had it not been for the help and advice of many faculty and students. I would like to thank Joel Solomon, Seth Bowser, Ian Campbell, Rob Passerotti, Nick Swanson, Briana Young, and Alexis Rowley for the time they have spent helping me grow as a researcher, and for always making the lab feel like my home away from home. I would also like to thank Joel, Seth, and Jerry Magraw for their contribution to the creation of SADPALM, our built-in-house Arduino controlled apparatus. A special thanks to Chuck Yeung, Darren Williams, and Natalie Mikita for their valuable advice and time. I also appreciate and thank the numerous people who gave me writing suggestions with the paper, and all of the researchers who came before me who brought the project to where it was when I started.

Most of all, I would like to thank Bruce Wittmershaus for the countless number of hours he has spent working on this project and for giving me the opportunity to research with him over the last three years. He has spent a **tremendous** amount of time helping me grow as a researcher, student, and human being. He was instrumental in helping me take full advantage of the opportunities available to me at Penn State Behrend, and he has gone above and beyond what is expected of a faculty member.

This material is based upon work supported by the National Science Foundation under Grant Number NSF-ECCS-1306157. Additional support was received through undergraduate research grants awarded from Penn State Erie, The Behrend College.

Chapter 1

Introduction

Luminescent solar concentrators (LSCs) are typically sheets of glass or plastic doped with fluorescent materials that are used to convert solar energy into electrical power (Fig. 1). The fluorescent materials in an LSC absorb sunlight and convert it into fluorescence, redirecting the light. An LSC acts as a waveguide, causing most of the fluorescence to be trapped by total internal reflection and directed towards its edges like a fiber optic. Photovoltaic (PV) cells are optically adhered to the edges and the fluorescence is absorbed and converted into electricity. Though they are not as efficient in converting sunlight into electricity as PV cells alone, LSCs low cost compared to PV cells make them attractive as a concentrator for potentially lowering the cost per kW/hr of solar power [Assadi et al., 2016; Debije and Verbunt, 2012; Shanks et al., 2016].

Not all of the sunlight that is incident on an LSC ends up as photons concentrated onto the PV cells. The absorption spectra of fluorescent materials is strongly wavelength dependent and may be limited to a small part of the UV/visible/NIR spectrum. This limited absorption bandwidth hinders the amount of sunlight converted into electricity. The limited absorption bandwidth is actually an advantage in some applications, such as when LSCs are used in greenhouses [Corrado et al., 2016] or windows [Zhao et al., 2014]. Increasing the optical density of an LSC increases its power output to an extent. Unfortunately, there is typically some overlap in the absorption and fluorescence spectra causing re-absorption losses that create a practical limit for an LSC's maximum concentrating ability [Debije and Verbunt, 2012; Wilson et al., 2010]. Depending on the optical density of the material, some of the light passes through an LSC

by either transmission of unabsorbed sunlight or through escape-cone losses of the fluorescence [Assadi et al., 2016; Debije and Verbunt, 2012; Hermann, 1982; Wilson et al., 2010].

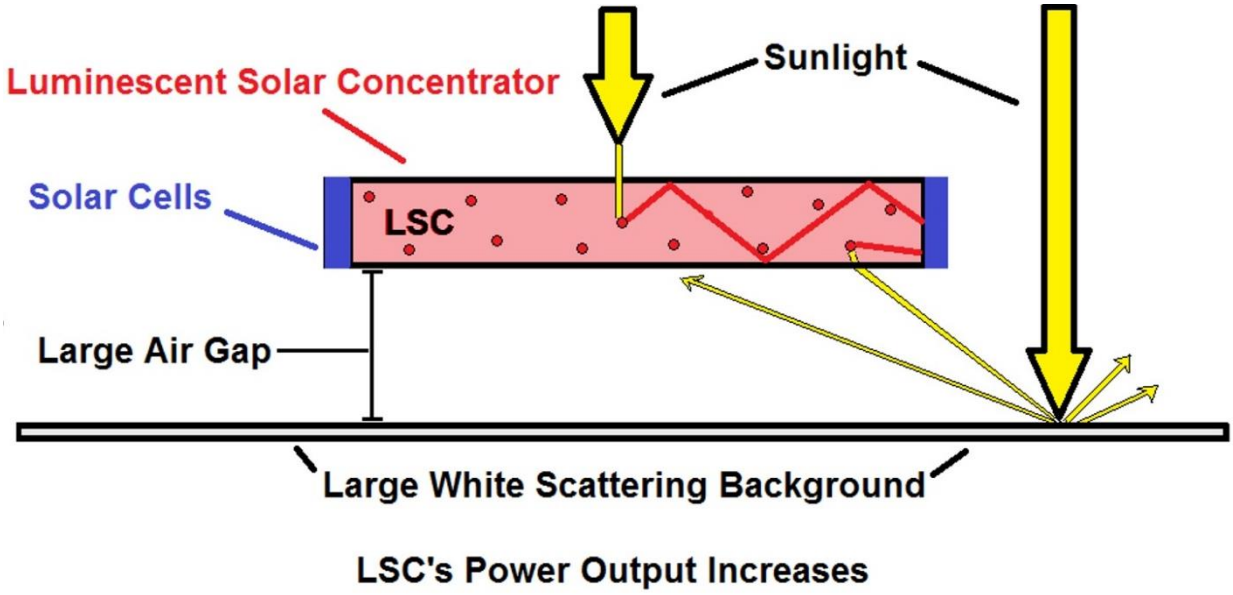

Figure 1: An LSC Using a Large White Background

A diagram of an LSC using a large white background to generate electricity by absorbing sunlight. The LSC contains fluorescent materials that absorb and redirect sunlight to its edges in the form of fluorescence. Solar cells along the edges absorb the fluorescence and generate an electric current. Some of the light incident on the LSC passes through, so an inexpensive white scattering background is placed underneath to scatter it back into the LSC. This work is unique in that the white backgrounds are made larger than the LSC. This allows light to shine directly on the larger background without being shaded by the LSC. The larger background scatters more light into the LSC, and is optimized when spaced by some optimal air gap.

An inexpensive reflective material underneath the LSC helps by sending this light back through the LSC for a second chance of absorption [Lifante et al., 1983; Roncali and Garnier, 1984]. Typically, a diffusive scatterer works better than a mirror [Debije et al., 2009]. Sunlight hitting an LSC at a small incident angle travels a short pathlength through the LSC making it less likely to be absorbed. On average, a diffusive scattering surface sends this transmitted light back into the LSC at larger incident angles, resulting in more internal reflection and longer pathlengths. This increases the light's chances of being absorbed more than if specular reflection

off a mirrored background occurred. Except for small LSCs, a highly reflective, diffuse scattering surface separated from the bottom of an LSC by an air gap is better than making optical contact between the scattering material and the LSC [Debije et al., 2009]. In the latter case, the scattering material can scatter the fluorescence trapped in the plate into angles that allow some of it to refract out of the plate.

Recent studies restricted their research to diffusive scattering surfaces, or white backgrounds, with the same area as the LSC. The backgrounds either were in direct contact with the LSC or spaced away from it by only a small air gap. Different small area elements around the white background were found to contribute different amounts to increasing the LSC's current [Debije et al., 2009]. The enhancement ratio for current generated by an LSC with a white background versus the size of the LSC initially dropped as the LSC's area increased and then remained nearly constant [Wang et al., 2010].

In this work, we explore the potential of a new, unique role for the white background by expanding it beyond its conventional configuration. We examine the benefits of using white backgrounds that are larger in area than the LSC, thereby partially capturing sunlight from a larger region. Experimental measurements and a computational model show how increasing the area of the diffusive white background and varying the air gap can dramatically increase the LSC's power output using inexpensive materials.

Chapter 2

Experimental Methods

The LSC used in these experiments was a 12.5 cm x 12.5 cm x 0.68 cm poly(methyl methacrylate) plate (index of refraction =1.48) (Fig. 2) infused with the fluorophore Lumogen F Red 300 (BASF). The plate has an optical density of 2.76 at its absorption peak of 577 nm [Hyldahl et al., 2009]. After cutting the plate, the edges were polished. PV cells (SolarMade) were cut and attached to all four edges using a clear optical adhesive (Norland 68T) such that they did not extend above or below the LSC's edges. The PV cells were electrically connected in parallel.

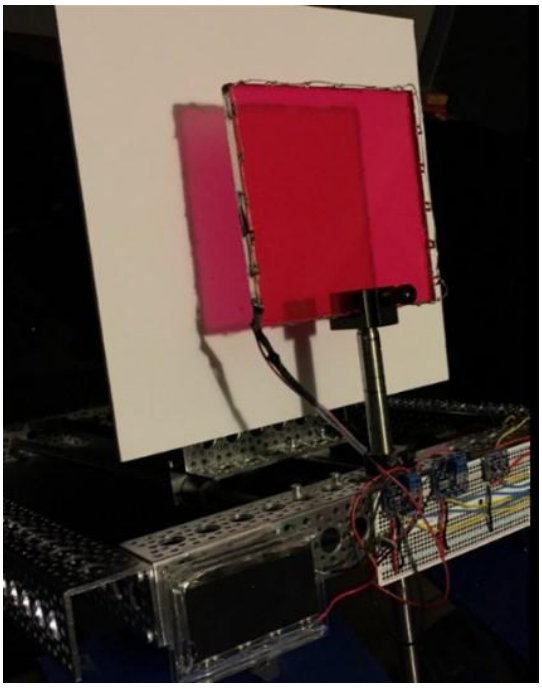

Figure 2: Experimental Apparatus

Apparatus for varying the distance between the luminescent solar concentrator (LSC) and a white background. The LSC is held in a fixed position at normal incidence to the sun while the air gap is varied by mounting the white background to the linear translational stage. The white background shown is four times (4x) the area of the LSC and has regions that are shaded (red region, same size as 1x area) and unshaded (outer white frame) by the LSC. Current from a reference PV cell (bottom center) is used to correct for small variations in the sun's irradiance.

Eight square white background plates of different areas were cut out of 5-mm thick foam poster board that had a white paper surface. The surface's reflectivity at 633 nm was 83% when compared to measurements from a plate of Spectralon (Labsphere) with a known reflectivity of

99% at 633 nm. The white paper surface acted as a Lambertian reflector when measured with a calibrated radiometer (International Light Technologies) over incident angles from 10° to 80°. The sides of the backgrounds had lengths of 12.5 cm (1x LSC area), 14.4 cm (1.33x LSC area), 16.1 cm (1.66x LSC area), 17.7 cm (2x LSC area), 21.7 cm (3x LSC area), 25.0 cm (4x LSC area), 35.4 cm (8x LSC area), and 50.0 cm (16x LSC area). The LSC was also tested with no white background such that light scattered off the distant environment could enter through the bottom of the LSC.

A programmable, microcontroller-based linear translational stage was designed and built in-house to hold the LSC and the white background being tested (Fig. 2). It varied the distance between the back surface of the LSC and the front surface of the white background, referred to as the air gap, from 0.7 to 19.0 cm. While the air gap was changed, the short circuit currents from the LSC and from the 6.7 x 3.2 cm reference PV cell mounted on the apparatus were measured simultaneously every ~3 ms for ~42 seconds. Approximately 14,000 data points per measurement were recorded, or one data point every ~13 μs. For each white background area, at least three consecutive measurements of the LSC's power output versus air gap were recorded and averaged to generate a final data curve (Fig. 3). The mean absolute deviation (MAD) averaged over an entire curve was 0.8 mW or less for all the curves. The measurements were done on a clear day between about 12:00 pm -1:00 pm. The irradiance of sunlight was a stable (81 ± 2) mW/cm^2 as measured using a calibrated radiometer (International Light Technologies). The current measured from the reference cell was used to correct the data for variations (~2%) in the sun's intensity. Using a digital multimeter, the open circuit voltage of the LSC was measured at (0.50 ± 0.01) V across the full range of current values for all measurements. This agrees with

the manufacturer's specification for the PV cells. The LSC's power output was calculated by multiplying the short circuit current by 0.50 V.

During each measurement, the white background was secured to the translational stage such that its surface was parallel and centered with respect to the surface of the LSC. The apparatus was then adjusted to set the LSC, white background, and reference cell surfaces at normal incidence to the sunlight. As the white background moved away from the LSC, the position of the LSC's shadow on the white background remained fixed, keeping a constant "shaded region" on the white background that is the same area as the LSC. The apparatus was designed to minimize the shadow created by the structure holding the LSC plate (Fig. 2). The C-Clamp holding the LSC caused the minimum air gap to be 0.7 cm rather than 0 cm. This was preferred over edge mounting of the LSC, which would have created a larger shadow on the white backgrounds.

Chapter 3

Experimental Results

3.1 Total white background

Experimental data showing how the LSC's power output changes with the size of the air gap using eight different white backgrounds are shown in Fig. 3. The LSC's power output using no white background is nearly constant with an average value of 406.7 mW and an average MAD of 0.3 mW over the time of the measurements. When any white background is placed behind the LSC with the smallest air gap (0.7 cm), the LSC's power output significantly increases compared to no white background being present. Using the 1x LSC area white background, the LSC's power output increases 16.2% from 406.7 mW to 473 mW. Increasing the white background's area to 1.33x, 1.66x, and 2x further increases the LSC's power output to 495, 505, and 508 mW, respectively. Any additional increase in the white background's area does not yield any more power with an air gap of 0.7 cm.

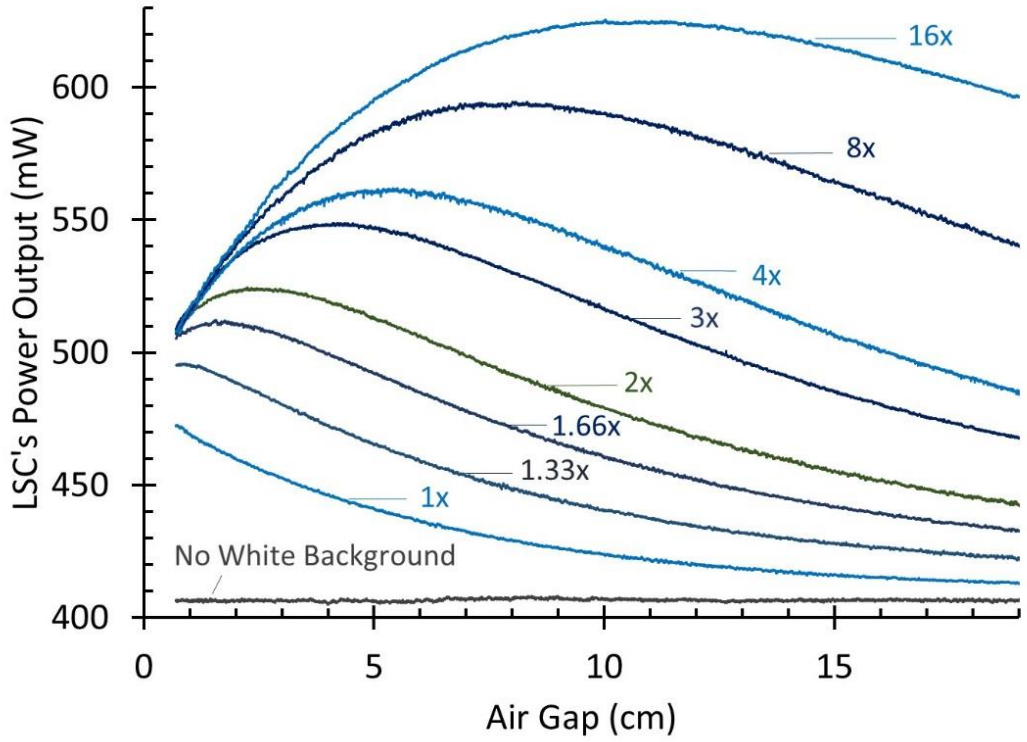

Figure 3: LSC's Power Output vs. Air Gap

LSC's power output vs. the air gap between the back of the LSC and a white background. The curve closest to the x-axis is data taken with no background behind the LSC. Each curve going further away from the x-axis represents successively larger backgrounds. The background areas are represented relative to the area of the LSC (156.25 cm^2). For example, 2x represents a square white background of area 312.5 cm^2.

As the air gap increases from 0.7 cm, the profile of the data for the LSC's power output versus air gap is different for each white background (Fig. 3). The LSC's maximum power output measured for the 1x white background occurs as soon as data recording begins (air gap of 0.7 cm). As the air gap increases for the 1x white background, the LSC's power output decays in an exponential fashion and approaches the LSC's power output when no white background is present. The data for the LSC's power output vs. air gap using the 1.33x-16x white backgrounds initially rise as the gap increases, reach a maximum power, and then slowly decay as the air gap further increases. The air gap that causes the LSC to produce the most power for a particular total white background is referred to as the optimal air gap.

The LSC's maximum power output increases as the white backgrounds get larger (Fig. 4). The LSC's maximum power output versus white background area fits well to a logarithmic trend line illustrating a decreasing return in the LSC's maximum power output per unit area of white background as the area increases. The trend line is not linked to any theoretical model, but does represent the general trend of the data and is suitable for extrapolating to white background areas larger than the LSC that were not tested. The LSC's maximum power output was 625 mW using the largest white background tested (16x) when separated by an optimal air gap of 10.7 cm. The LSC's maximum power output using the 16x white background is 28% and 54% larger when compared to the LSC's maximum power output using a 1x white background and no white background, respectively. Since the 1x white background curve (Fig. 3) does not have a defined critical point (maximum), it was assumed that 0.7 cm might not be its optimal air gap. The trend line (Fig. 4) was used to estimate the LSC's maximum power output using a 1x area background. It predicted a value of 487 mW which is only 14 mW higher than the 473 mW measured at an air gap of 0.7 cm (Fig. 3).

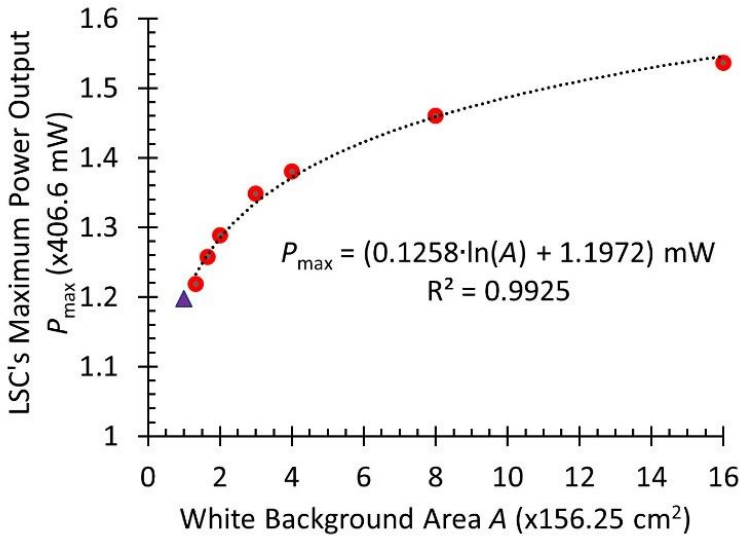

Figure 4: LSC's Max Power vs. White Background Area

The LSC's maximum power output relative to the power for the no background case (406.6 mW) as a function of the area of the white background for areas 1.33x-16x (circles). To illustrate the trend of the data, it is fit to a function (dotted line). This trend line is used to estimate the maximum power output for the 1x white background if data could have been recorded for air gaps less than 0.7 cm (triangle).

For the 1.33x white background and larger, the optimal air gap increases as the area of the white background increases (Figs. 3 and 5). The optimal air gap versus white background area fits well to a logarithmic trend line (Fig. 5). This trend line is not linked to a theoretical model but can be used to predict the optimal air gap for white backgrounds larger than the LSC that were not tested.

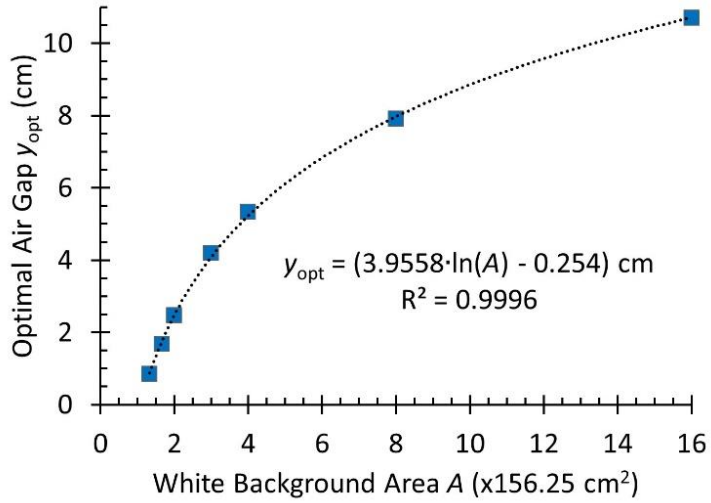

Figure 5: Optimal Air Gap vs. White Background Area

The optimal air gap between the LSC and its total white background for areas 1.33x-16x (squares). The optimal air gap causes the LSC's power output to be at a maximum using a particular area white background (Fig. 3). To illustrate the trend of the data, it is fit to a function (dotted line).

To accurately determine the optimal air gap and the LSC's maximum power output for each white background, all data within $\pm$3 cm of the estimated optimal gap (Fig. 3) were fit to a second-order polynomial (not shown). The optimal air gap was determined using the second order polynomial's first derivative. This optimal air gap was then used in the second-order polynomial to calculate the value for the LSC's maximum power output (values in Fig. 4).

3.2 Unshaded region of the white background

Because the experiments occurred at normal incidence, the "shaded region" is the red shadowed area directly under the LSC (Fig. 2). This is equivalent in area to the 1x white background. The 1x white background curve in Fig. 3 is the shaded region's contribution to the LSC's power output versus the size of the air gap. The "unshaded region" is the bright white area

larger than the 1x white background (Fig. 2). To understand how the unshaded region of a white background contributes to increasing the LSC's power output, the LSC's power output using the 1x background was subtracted from each curve for backgrounds larger than 1x (1.33x-16x, Fig. 3) and plotted in Fig. 6. For example, the 2x curve is the 2x curve minus the 1x curve from Fig. 3. The 2x curve in Fig. 6 represents only the contribution of the unshaded region of the 2x white background to the LSC's power output. The curves representing the 1.33x-16x unshaded backgrounds' contributions to the LSC's power output as a function of air gap are similar to their corresponding curves for the total white backgrounds (Fig. 3). The curves in Fig. 6 have distinct maxima that occur using air gaps greater than the optimal air gaps observed in the corresponding curves of the total white backgrounds in Fig. 3.

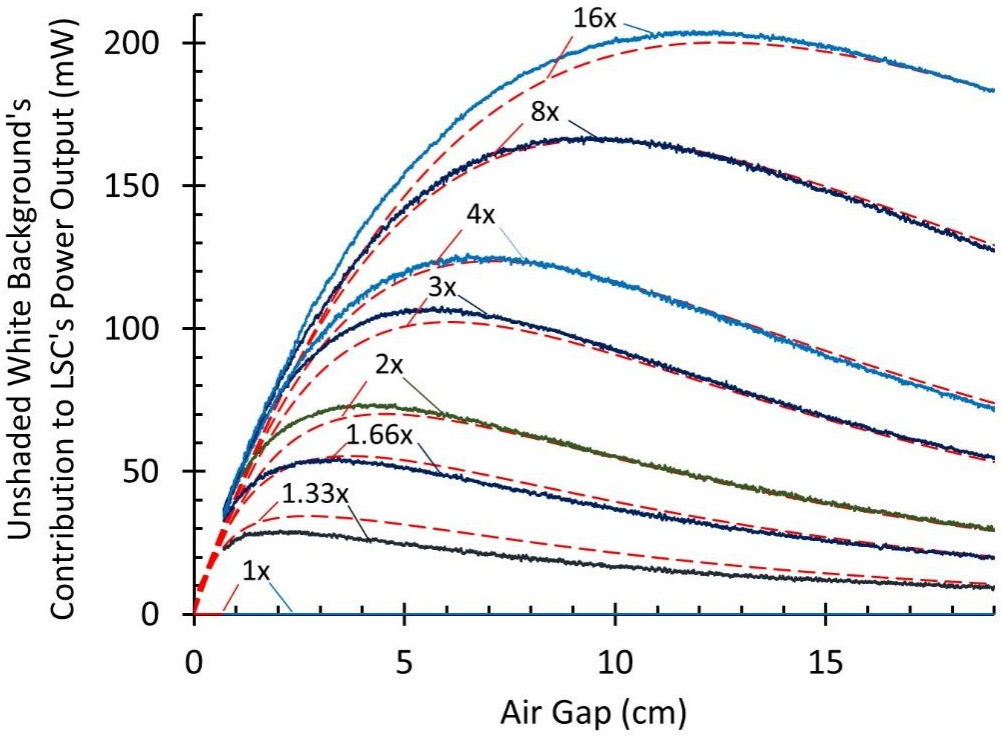

Figure 6: Power Contribution from Unshaded White Background vs. Air Gap

The LSC's power output due to scattered light it receives only from the unshaded region of the white background as a function of the air gap for backgrounds of area 1x-16x (solid lines indicate measured data). The unshaded region of the background is the white area that extends beyond the shadow cast by the LSC (area greater than the 1x white background) (Fig. 2). The 1x white background has no unshaded region, so it contributes zero on this plot. Plots of the theoretical power outputs of the LSC (dashed lines) due to light leaving the unshaded white background for backgrounds of area 1x-16x are also shown near their respective experimental curves.

Chapter 4

Computational Modeling: Normal Incidence

4.1 Modeling of the total unshaded region

Also in Fig. 6 are the predictions of a computational model, which compare favorably to the experimental results of the unshaded white backgrounds' contributions to the LSC's power output. The model provides insight into why increasing the air gap causes an LSC to produce more power and how the optimal air gap changes with the white background's area. The model approximates how much light is scattered off the unshaded region of the white background and is transmitted into the LSC. The white background's area and the air gap were varied to determine how these parameters affect the photons per second transmitted into the LSC. The model uses basic optical considerations and assumes the LSC's power output due to the unshaded white background is proportional to the total number of photons per second P_{WL} entering the underside of the LSC.

The number of photons per second leaving an area of the white background P_w is equal to the incident photons per second per area from the sun I_S multiplied by a small area of the white background ΔA_W and a loss constant C. P_w is also equal to the outgoing photons per second per area leaving the white background I_w integrated over the area of a semi-sphere of light with radius r that is centered on ΔA_W.

$$P_w = \int_0^{2\pi} \int_0^{\pi/2} I_W r^2 \sin\theta d\theta d\varphi = C I_S \Delta A_W \quad (1)$$

Assuming the white background is a Lambertian surface (Pedrotti and Pedrotti, 1993),

$$I_W = I_{W0} \cos\theta \quad (2)$$

where θ is the angle from the normal of the white background's surface to the ray of scattered light, and I_{W0} is I_W at $\theta = 0$. Placing Eq. (2) into Eq. (1) and solving gives:

$$I_{W0} = \frac{CI_S \Delta A_W}{\pi r^2} \quad (3)$$

Using this in Eq. (2) results in:

$$I_W = \left(\frac{CI_S \Delta A_W}{\pi}\right) \frac{\cos\theta}{r^2} \quad (4)$$

The number of photons per second incident on a small area on the underside of the LSC is equal to I_w multiplied by the small area element of the LSC ΔA_L and by another $\cos\theta$ due to the cross-sectional area of the LSC relative to the incident light. Only a fraction T of these photons are transmitted into the LSC while the rest are reflected off the surface as described by Fresnel's Equations. P_L, which is the total number of photons per second from ΔA_W entering ΔA_L on the LSC is given by:

$$P_L = \Delta A_L I_W \cos\theta \, T = \left(\frac{CI_S \Delta A_W \Delta A_L}{\pi}\right) \frac{\cos^2\theta}{r^2} T \quad (5)$$

The transmittance T (average for randomly polarized light) is,

$$T = 1 - \frac{1}{2}\left[\left(\frac{\sin(\theta-\theta_t)}{\sin(\theta+\theta_t)}\right)^2 + \left(\frac{\tan(\theta-\theta_t)}{\tan(\theta+\theta_t)}\right)^2\right] \quad (6)$$

where θ_t is the angle of transmittance (Pedrotti and Pedrotti, 1993). Using Snell's law, $\theta_t = \arcsin\left(\frac{\sin\theta}{n}\right)$, where n = index of refraction of the LSC material (1.48 for this experiment) and the index of air is assumed to be one. For the numerical integration, Eq. (5) was evaluated using an *xyz* coordinate system where *y* is the air gap and the white background is in the *xz* plane. The *x* coordinate is the distance along the x axis from the center of ΔA_W to the center of ΔA_L and similarly for *z*. The substitutions are, $r = \sqrt{x^2 + y^2 + z^2}$ and $\cos\theta = \frac{y}{\sqrt{x^2+y^2+z^2}}$ which change Eq. (5) to:

$$P_{\mathrm{L}} = \left(\frac{CI_{\mathrm{S}}\Delta A_{\mathrm{W}}\Delta A_{L}}{\pi}\right)\frac{y^2}{r^4}T = \left(\frac{CI_{\mathrm{S}}\Delta A_{\mathrm{W}}\Delta A_{\mathrm{L}}}{\pi}\right)\frac{y^2}{(x^2+y^2+z^2)^2}T \quad (7)$$

The calculation of P_{WL} is done numerically while keeping the air gap and area of the white background held constant. The unshaded white background and the LSC are divided into many finite area elements ΔA_W and ΔA_L. For a particular ΔA_W, P_L is calculated using Eq. (7) for every ΔA_L on the LSC and summed together. The process is repeated and summed over all ΔA_W's to give P_{WL}. P_{WL} is the number of photons per second into the LSC from the entire unshaded white background at an air gap of *y*. ΔA_W and ΔA_L were set at 0.1 x 0.1 cm after progressively decreasing them in size until no significant change was observed in the result. P_{WL} versus air gap for each area of unshaded white background is generated by varying the air gap from 0 to 19.0 cm in steps of 0.1 cm.

As shown, the model uses only the area and index of refraction of the LSC. It does not use, and is independent of its thickness and absorption spectrum and other factors relating the complicated processes through which the scattered light is absorbed, fluoresced, guided through the LSC, and ultimately converted into electrical power. We are assuming that the model's results are proportional to the observed power from the LSC and that the model contains the key elements for predicting how that power varies with the size of the unshaded white background and the air gap. The model estimates how much scattered light from the unshaded white background is transmitted into the LSC, but it does not calculate the actual values for the power generated by this light. To compare the model's results with the experimental data (Fig. 6), all the theoretical curves need to be multiplied by a normalization constant**.** This constant was chosen as the number needed to normalize the 8x experimental data to the 8x theoretical prediction with an air gap of 10.0 cm. This value was chosen because when it was applied to all

of the theoretical curves, they agreed well with the experimental results using air gaps of 0.7 cm and 19.0 cm; where the experimental data started and ended. The theoretical curves are likely comparable to what the model would predict for other sizes of square LSCs and white backgrounds, though the exact optimal air gaps may change depending on the fluorescent material used and the size and optical density of the LSC.

4.2 Modeling of the unshaded region broken up into frames

To understand the relative contributions to the LSC's power output from regions of the white background farther away from the background's center, the unshaded region of the 8x area white background was broken up into square frames of equal widths (Fig. 7).

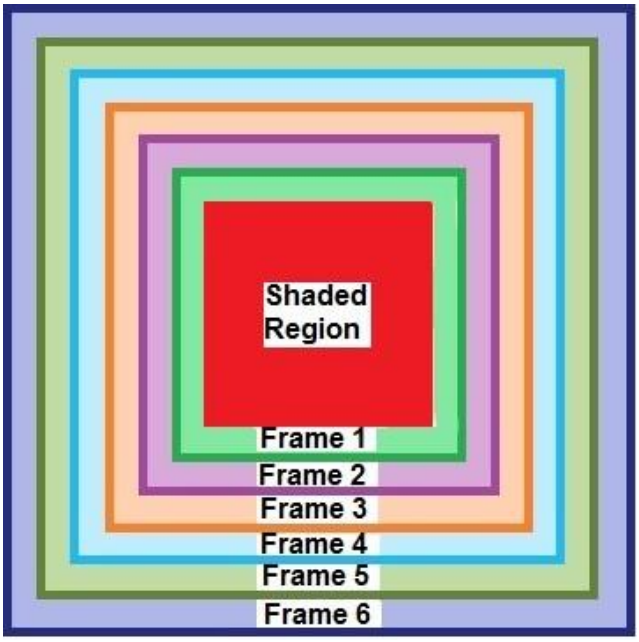

Figure 7: Diagram of 8x White Background Broken Up Into Frames

Breaking the unshaded white background into frames. The unshaded region of the 8x area white background is split into 6 square "frames" all with widths of 1.905 cm and labeled with increasing value as the frame is found further from the center of the white background (also center of the shaded region).

The theoretical model determined each frames contribution to the LSC's power output as a function of the air gap (Fig. 8). The same normalization constant was used as described earlier to convert the theoretical curves into the LSC's power output in mW. The model predicts that the air gap causing the LSC's highest power output (due to one frame) increases as the frame moves further from the center of the white background. Although a frame's area increases the further it gets from the center of the background (Fig. 7), its maximum contribution to the LSC's power output actually decreases (Fig. 8). When the air gap is small, the frames further from the center of the white background provide no additional power. The sum of the power contributions from all of the frames is in agreement with the model's calculation for the total unshaded region of the 8x background.

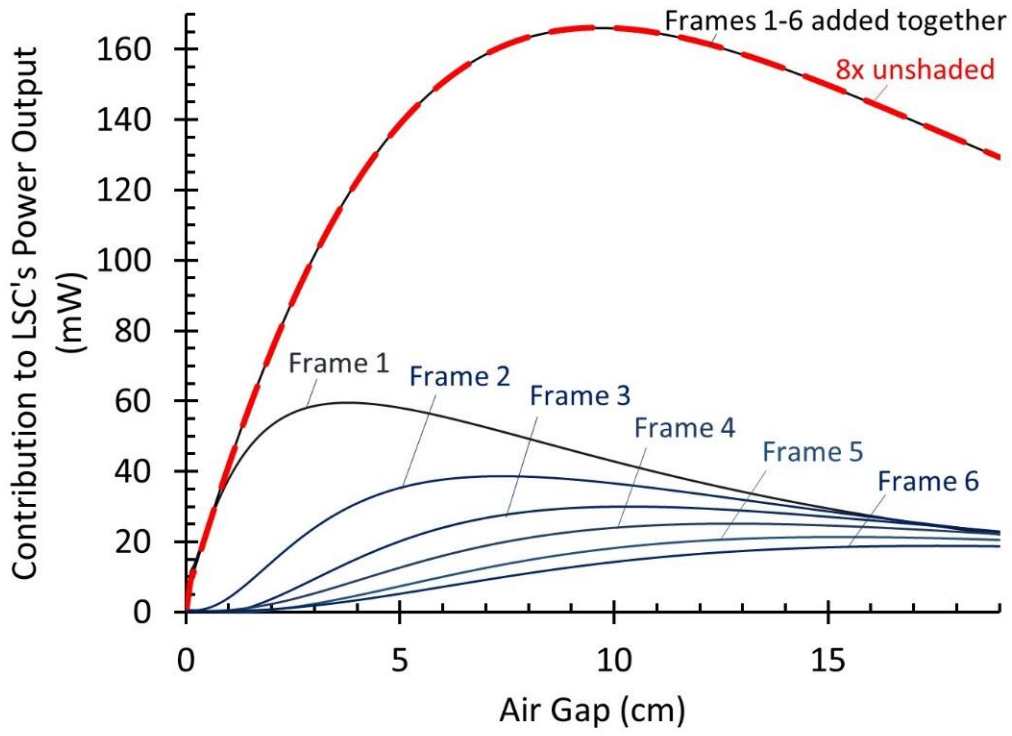

Figure 8: Power Contributions from Various Frames of the 8x White Background

Results calculated from the theoretical model show how much the scattered light from each frame (1-6, Fig. 7) of the unshaded region of the 8x white background contributes to the LSC's power output (six labeled solid lines closest to the x axis). To show consistency, the program's results for the total unshaded region of the 8x white background (dashed line, also shown in Fig. 6) is compared to the sum of the calculated results for frames 1-6 (solid line).

Chapter 5

Discussion: Normal Incidence

5.1 1x white background

The LSC's power output with a white background of the same area separated by a 0.7 cm air gap is 16.2% more than when no white background is present (Fig. 3). This is projected to be a 19.7% improvement if the white background is very close to the LSC without interfering with total internal reflection. These results are in agreement with those of previous studies for a 1x diffusive scattering background separated by a small air gap, which have also observed improvements in the LSC's power output [Debije et al., 2009; Wang et al., 2010]. The benefit of using a white background is sensitive to the LSC's optical density, absorption and fluorescence spectra, size, and shape [Debije et al., 2009]. The optical density and size of the LSC used in this study were not adjusted to optimize the LSC's power output using a 1x white background, although it is similar to LSCs used in previous studies [Debije et al., 2009; Desmet et al., 2012].

5.2 Why larger air gaps benefit larger white backgrounds

When exposed to sunlight of normal incidence, an LSC's power output can be increased beyond the 1x white background result if the white background is larger than the LSC (Figs. 3 and 3) and it is spaced an optimal distance away (Fig. 3 and 5). The unshaded white background region (bright white Fig. 2) receives the sun's full irradiance, which is considerably more than the light transmitted through the LSC that illuminates the shaded region (red shadow). Though the sunlight coming off the unshaded region is scattered in all directions, a significant portion

can reach the bottom of the LSC if there is space between the bottom of the LSC and the white background.

Intuitively, it makes sense that white backgrounds larger than an LSC need to be separated from an LSC in order for the unshaded region to have a contribution. If there were no air gap, scattered light from the unshaded region would have no path to reach the bottom of the LSC. This is evident in Fig. 3 where data for the LSC's power output for each area white background appear to converge as the air gap goes to 0 cm. This is also supported by the results of the theoretical model, showing that all of the unshaded backgrounds' contributions go to 0 mW as the air gap goes to 0 cm (Fig. 6).

As the air gap is increased, there is a balance reached between the losses and gains controlling the amount of scattered light reaching the LSC from the shaded and unshaded regions. Some insights into the interplay between the air gap, area, and the unshaded white background's contribution to the LSC's power are evident in the model (Eq. 7). The normalized curves from the model predict the general behavior of the LSC's power output when the air gap and the areas of the unshaded white background are varied (Fig. 6). This includes the presence of an optimal air gap, though the model's predictions are at slightly larger separations than those observed experimentally.

With a 0.7 cm air gap, the 2x and larger white backgrounds contribute the same amount to the LSC's power output (Figs. 3 and 6). Scattered light from the unshaded region beyond the area of the 2x white background is weakened by the inverse square law and the light's large angles of incidence with the LSC. With an air gap of 0.7 cm, the outer frames of the unshaded white backgrounds contribute little (if at all) to the LSC's power output. Fig. 8 clearly illustrates

that only the closest frame (frame 1) scatters any appreciable light into the LSC for air gaps less than 1 cm.

The contribution of the unshaded region of a white background to the LSC's power output can be pictured as a summation of the power contributions from a nearly infinite number of very thin frames. For any given air gap, only one of these thin frames is optimized to contribute the most it can to the LSC's power output. The thin frames closer or further from the center of the white background do not contribute their maximum possible values. For example, the total unshaded region of the 8x white background has a maximum contribution to the LSC's power output with an air gap size of 9.6 cm (Fig. 6 and 8). With an air gap of 9.6 cm, the slopes of the power contributions from the outer most frames (3, 4, 5, and 6) are positive while the slopes of inner frames (1 and 2) are negative (Fig. 8). If the air gap increases above 9.6 cm, frames 1 and 2 will contribute less and frames 3, 4, 5, and 6 will contribute more.

The overall optimal air gap is determined by a summation over the contributions of the shaded region and each individual frame of the unshaded region of the white background. As the white background gets larger, the contributions from the outer frames of the unshaded background increase the optimal air gap (Figs. 3 and 5). As a frame gets further from the center of the white background, its contribution to the LSC's power decreases (Fig. 8) even though its area is increasing (Fig. 7). These diminishing returns in the LSC's power output per area of white background are reflected in the logarithmic trend line that fits the experimental data (Fig. 4).

5.3 Significance of the unshaded region

The unshaded region's contribution to the LSC's power can be considerable given the difference in the sun's irradiance on the shaded and unshaded regions of the white background. For example, with an optimal air gap, the 1x background is projected to contribute 80 mW more than the LSC's power output observed for the no background case (Fig. 4). The 2x white background has equal parts of shaded area and unshaded area. Considering only the unshaded region of the 2x white background, the highest amount it contributes to the LSC's power output is 73 mW with an air gap of 4.2 cm (Fig. 6 experimental data). With an air gap optimized for the unshaded region, scattered light leaving the unshaded region can cause the LSC to produce nearly the same amount of power as the shaded region does with a very small air gap. This happens despite the unshaded region being further away from the LSC and having larger average angles of incidence than light from the shaded region. The white background frames surrounding an LSC (unshaded region at normal incidence to the sun) can contribute substantially to the LSC's power output without obstructing the view through the LSC if the 1x area background directly below the LSC is not present. In this way, LSCs proposed as windows that do not absorb visible light [Zhao et al., 2014] could benefit from a surrounding frame of white background material on the building. An open window pushed out away from the building could have sunlight scattered off the white frame reach the underside of the LSC, increasing its power output.

5.4 Reducing cost

Anticipating a relatively low cost for adding a white background to an LSC points to a promising path for reducing the cost per kilowatt produced by an LSC. The ideal background size would come from a cost analysis considering the LSC's additional power output per area of white background, the additional cost of the background and its mounting, and the amount of space available for the system. The decreasing slope as the background's area increases in Fig. 4 indicates there are diminishing returns for each increase in the white background's area. Additional cost saving would be realized from a system made of a very large white background under an array of many smaller LSCs optimally separated and spaced above the background. In such a design, considerably more of the sunlight scattered off the white background could be collected compared to the single LSC system described in this work.

Chapter 6

Computational Modeling: Varying Angle of Incidence

6.1 Making the model

Preliminary experimental data suggests that the optimal air gap changes as the angle of incidence of the sunlight varies. The primary cause for this change is most likely the change in the location of the LSC's shadow (the shaded region) on the white background. At normal incidence, the location of the shaded region does not change as the size of the air gap is increased (Fig 9). When the sunlight is not at normal incidence, the shaded region's location and size on the white background change as a function of the air gap (Fig. 10). As the air gap increases, more of the background directly underneath the LSC becomes unshaded and receives the full intensity of the sun. The computational model was improved to predict how the LSC's power output would behave as a function of the size of the air gap, the white background's area, and the sunlight's angle of incidence on the system.

The new computational model works very similarly to the previous version, however there are some changes which must be made to model the system at angles of incidence other than 0^o. The model still assumes that the white background is perfectly Lambertian, and that there is no specular reflection off its surface for any angle of incidence. There is also the assumption that the shaded region moves linearly (Fig. 10) across the background as the air gap is increased. There are regions to the left and right of the shaded region which are completely devoid of light (black region in Fig. 10) due to the solar cells along the edge blocking the sunlight. The size of the black regions and the shaded region grow larger as the angle of

incidence is increased. The sizes of these regions can be calculated using geometric arguments and Snell's Law of Refraction for each angle of incidence.

The same normalization constant used in the previous model quantifies the conversion of light entering the LSC from the unshaded region at normal incidence (white region in Fig. 10 and 11). A different normalization constant is needed to convert light entering the LSC from the shaded region (the light red region on the background in Fig. 9 and 10). This shaded region's normalization constant was determined by fitting the model's results to the experimental results for the 1x background at normal incidence with an air gap of 10.0 cm. The shaded region's normalization constant at normal incidence is 14% of the unshaded region's normalization constant.

As the angle of incidence increases from normal incidence, the shaded region (when it is on the white background), gets darker. This causes a decrease in the shaded region's normalization constant as the angle of incidence increases. The shaded region gets darker because of the increase in reflections off the air-to-LSC interface and the LSC-to-air interface as described by Fresnel's equations. There is also a decrease in light reaching the shaded region due to an increase in pathlength through the material as described by Snell's Law of Refraction and the Beer-Lambert Law of Absorption. A third effect, which decreases both the unshaded and shaded regions' normalization constants, is the decreasing irradiance on the background described by the cosine of the incidence angle.

The computational model was used to predict the power contribution of a 1x background for angles of incidence between 0^o and 90^o while the air gap was varied from 0.1 cm to 10.0 cm (Fig.12). The angles of incidence were varied in 10^o increments and the air gap was varied in steps of 0.1 cm. The integration used area elements of 0.05 cm x 0.05 cm.

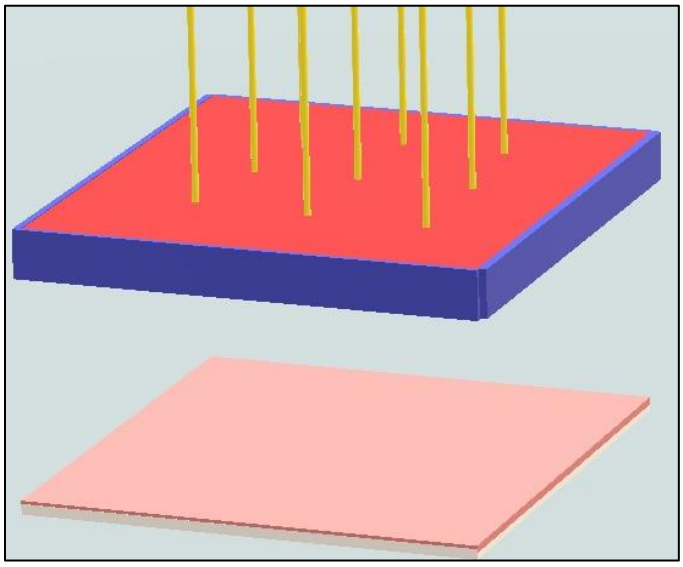

Figure 9: LSC with 1x Background at Normal Incidence

An LSC with a 1x background separated by an air gap of about 6 cm at normal incidence to the sun. The shaded region (light red) is exactly the size of the 1x background and covers the entire background for all air gap values.

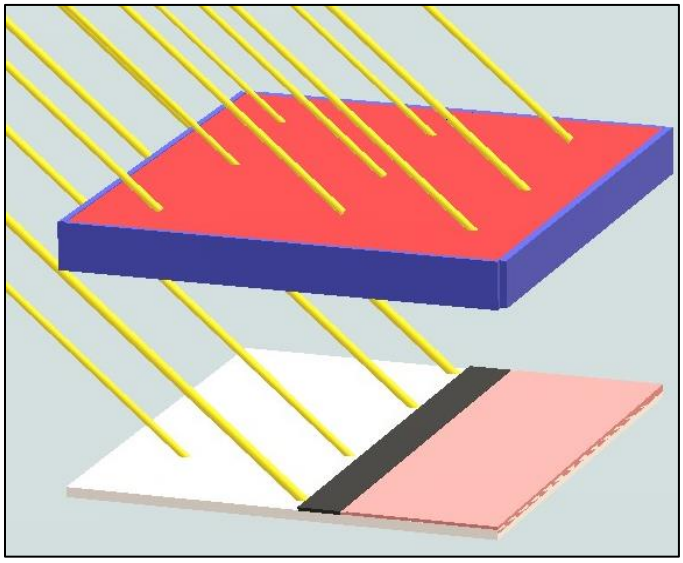

Figure 10: LSC with a 1x Background at 45º

An LSC with a 1x background separated by an air gap of about 6 cm at 45º incidence to the sun. The black (no light) and red shaded regions move to the right as the air gap increases, causing more of the background to become unshaded (white) and receive the full intensity of the sun.

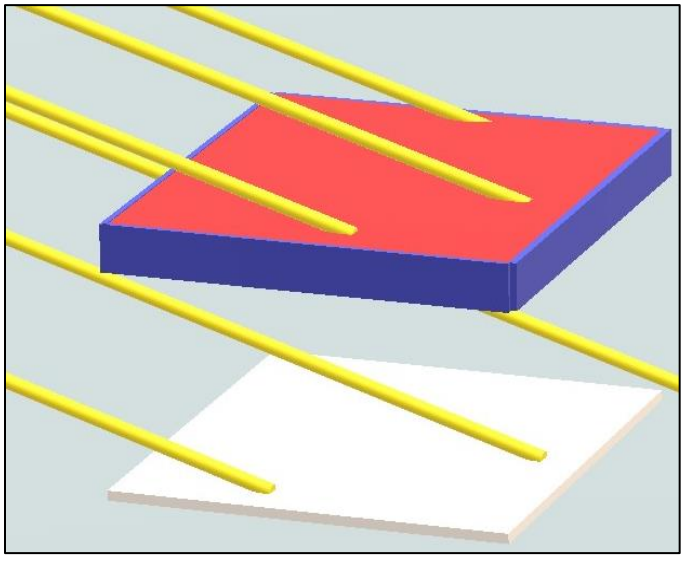

Figure 11: LSC with a 1x Background at 70º

An LSC with a 1x background separated by an air gap of about 6 cm at 70º incidence to the sun. The background is entirely unshaded because the black and red shaded regions are entirely to the right of the 1x background. The LSC will not benefit from any additional increase in the size of the air gap (Fig. 12).

6.2 1x background results

The results for the 1x background are shown in Fig. 12. There is no non-zero optimal air gap for angles of incidence between 0º and 20º. The 1x background was observed to have an optimal air gap between 30º and 80º which varied for each angle of incidence. The size of the optimal air gap increases then decreases as the angle of incidence gets larger. The 60º, 70º, and 80º curves have cusps that occur where the shadow leaves the background.

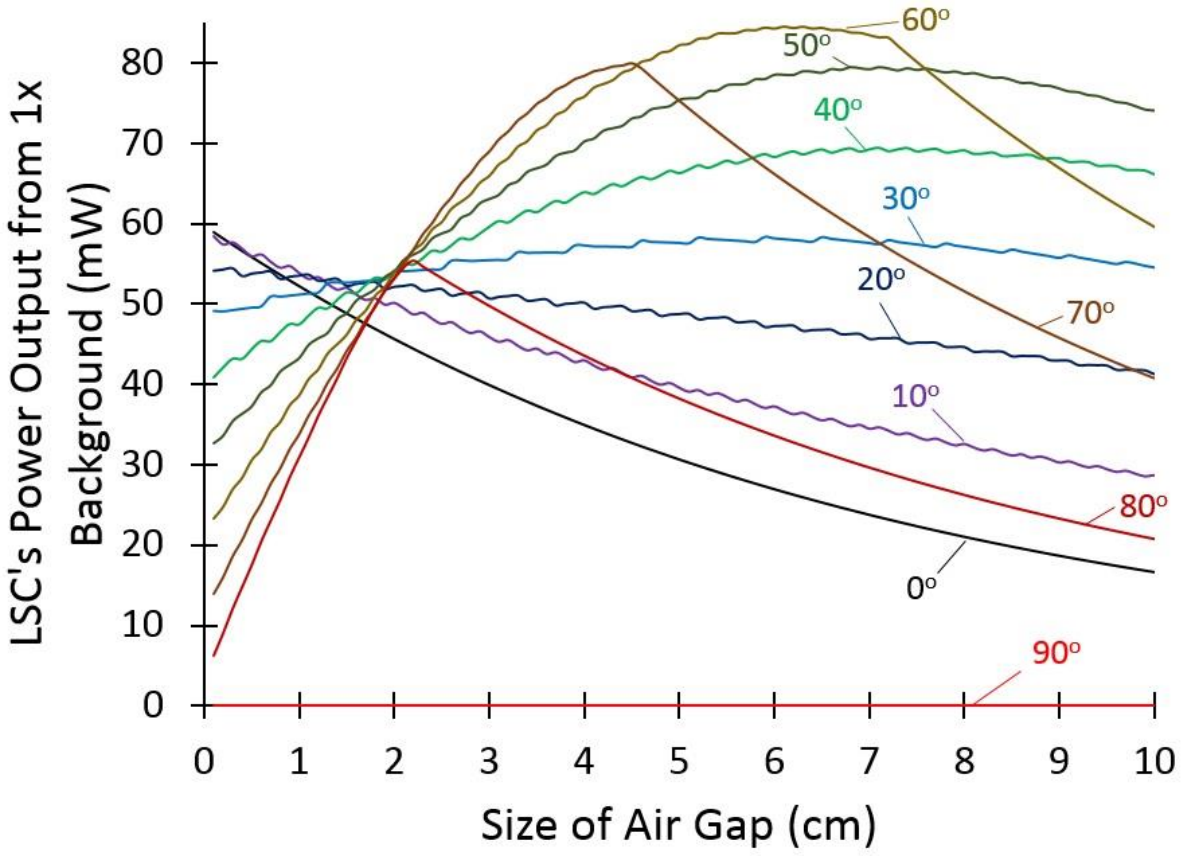

Figure 12: Power Contribution from 1x Background: Varying Angle of Incidence

The power contribution from a 1x background as a function of the size of the air gap. Each curve represents the LSC/background system being at a different angle of incidence relative to the sun. The model predicts that the optimal air gap changes with the angle of incidence. The cusps noticeable in the 60º, 70º, and 80º curves represent the air gap at which the shadow completely leaves the background. These cusps occur for smaller angles of incidence at larger air gaps than shown.

Chapter 7

Discussion: Varying Angle of Incidence

7.1 Why larger air gaps benefit a 1x background for large angles of incidence

The model predicts the 1x background's optimal air gap occurs at non-zero values for larger angles of incidence because of the shadow's changing location across the background. As the angle of incidence gets larger, the shadow moves off the background more quickly as the air gap is increased. This allows for the Sun to illuminate the background directly, causing a much brighter scattering surface to send light into the LSC. This background is directly underneath the LSC, which allows more of the scattered light to be transmitted into the LSC. Because the shaded region's normalization constant decreases at a faster rate than the unshaded region's normalization constant, the LSC benefits even more by increasing the air gap to reduce the area of the shaded region and increase the area of the unshaded region.

Cusps occur in the curves whenever the shadow completely leaves the background making the background entirely unshaded (Fig. 12). The cusps are only noticeable for the 60^{o}, 70^{o}, and 80^{o} curve because data is reported only up to a 10.0 cm air gap. The optimal air gap occurs before the cusps occur for angles of incidence 60^{o} and smaller. In other words, for angles including and below 60^{o}, the system is optimized when the shadow is still on the background. The 70^{o} and 80^{o} curves reach their optimal air gap when the shadows leave the background (at the cusps). This is strong evidence that the optimization occurs because the shadow is moving across the background. Once the shadow leaves the background and it is entirely unshaded, there is no further benefit to increasing the air gap and the power output decays very similarly to how it did at normal incidence when the background was entirely shaded.

7.2 Model vs. real life

It is important to note, as the model predicts that the power contribution from the 1x background is larger for angles of incidence between 40^o to 70^o than for normal incidence. At 70^o incidence, the sunlight's irradiance on the background is only 34% of what it is at normal incidence, yet at 70^o the optimal power contribution from the white background is 33% higher than the optimal power contribution at normal incidence. This is even more surprising because the optimal air gap at 70^o is 4.5 cm larger than at normal incidence. Experiments should be done to verify the results of the model, however there are assumptions in the model which will cause deviations from experimental results. It is unlikely that a real white background material will be perfectly Lambertian. The choice of white background and its specular reflection as a function of the angle of incidence would be an interesting optimization problem which I would encourage other researchers in the field to pursue. Additionally, there may be unforeseen issues with the choice of generalizing the entire shaded regions conversion to electrical power in the form of a single normalization constant. While the normalization constant seemed to agree very well with experimental results at normal incidence, the spectrum of the light scattering off of the unshaded and shaded regions are very different, and they are likely to interact with the LSC in different ways. It is important to track the photons when they enter the LSC from the shaded region to understand what percentage are being absorbed and fluoresced towards the solar cells and what percentage are being reflected directly towards the solar cells. The next step to improve the computational model would be use statistics and probability to trace individual photons through the system to optimize it.

The purpose of this model was to help describe how an LSC might be optimized in a scenario in which it is stationary and the Sun moves across the sky as it would during the day.

The most important result of this improved model is that it suggests that the moving shadow across the background as a function of air gap and angle of incidence could be an important variable in such an optimization problem.

Chapter 8

Conclusions

LSCs are dramatically improved by incorporating large diffusive white backgrounds and separating them from the LSC by a large air gap. The LSC's increased power output and the projected low cost of white backgrounds indicates an increase in cost efficiency. As the white background's area gets larger, the LSC's maximum power output increases and so does the size of its optimal air gap. An optical model agrees with my experimental findings and explains the effects leading to the optimization of an LSC using a larger white background separated by a large air gap when the sunlight is at normal incidence. The white background frames surrounding the LSC have a significant contribution to the LSC's power output when separated by an appropriate air gap. Using white background material around LSC windows could improve their performance. The improved computational model also predicts that the optimal air gap changes as the angle of incidence is varied. This is due to the changing position of the shadow on the background. The results of the improved show that there is more work to do. In summary, the use of larger white backgrounds can dramatically improve LSCs, but there is still work to be done to fully optimize the system in practical applications where the Sun's angle is allowed to vary.

BIBLIOGRAPHY

Assadi M.K., Hanaei H., Mohamed N.M., Saidur R., Bakhoda S., Bashiri R., Moayedfar M., 2016. Enhancing the efficiency of luminescent solar concentrators. Appl. Phys. A 122, 821-1-821-12.

Corrado C., Leow S., Osborn M., Carbone I., Hellier K., Short M., Alers G., Carter S.A., 2016. Power generation study of luminescent solar concentrator greenhouse. J. Renew. Sustain. Energy 8, 043502-1-043502-11.

Debije M.G., Teunissen J.-P., Kastelijn M.J., Verbunt P. P.C., Bastiaansen C.W.M., 2009. The effect of a scattering layer on the edge output of a luminescent solar concentrator. Sol. Energy Mater. Sol. Cells 93, 1345-1350.

Debije M.G., Verbunt P.C., 2012. Thirty years of luminescent solar concentrator research: solar energy for the built environment. Adv. Energy Mater. 2, 12-35.

Desmet L., Ras A.J.M., de Boer D.K.G., Debije M.G., 2012. Monocrystalline silicon PV luminescent solar concentrator with 4.2% power conversion efficiency. Opt. Lett. 37, 3087- 3089.

Hermann A.M., 1982. Luminescent solar concentrators – a review. Sol. Energy 29, 323-329.

Hyldahl M.G., Bailey S.T., Wittmershaus B.P., 2009. Photo-stability and performance of CdSe/ZnS quantum dots in luminescent solar concentrators. Sol. Energy 83, 566–573.

Lifante, G., Cusso, F., Meseguer, F., Jaque, F., 1983. Luminescent solar concentrators as bifacial captors. Sol. Cells 8, 355-360.

Pedrotti F.L., Pedrotti L.S., 1993. Introduction to Optics, second ed. Prentice Hall, Englewood Cliffs, NJ.

Roncali, J., Garnier, F., 1984. New luminescent back reflectors for the improvement of the spectral response and efficiency of luminescent solar concentrators. Sol. Cells 13, 133-143.

Shanks, K., Senthilarasu, S., Mallick, T.K., 2016. Optics for concentrating photovoltaics: Trends, limits, and opportunities for materials and design. Ren. Sus. Energy Reviews 60, 394-407.

Wang C., Winston R., Pelka D., Carter S., 2010, Size- and structure-dependent efficiency enhancement for luminescent solar concentrators. J. Photon. Energy 1, 015502-1-015502-8.

Wilson L.R., Rowan B.C., Robertson N., Moudam O., Jones A.C., Richards B.S., 2010. Characterization and reduction of reabsorption losses in luminescent solar concentrators. Appl. Opt. 49, 1651-1661.

Zhao Y., Meek G.A., Levine B.G., Lunt R.R., 2014. Near-infrared harvesting transparent luminescent solar concentrators. Adv. Opt. Mater. 2, 606-611.

Academic Vita of Jonathon R. Schrecengost

JonathonSchrecengost1996@gmail.com

Education:

Penn State Erie, The Behrend College, Erie, PA — Dean's List all semesters

Bachelor of Science in ***Physics*** — Schreyer Honors Scholar

Minors: Chemistry (29 credits), Computer Science, Mathematics, and Astrophysics (161 credits)

Research Experience:

Research Assistant- Experimental & Computational Solar Energy Research (May 2015-May 2018)

- Creating and optimizing luminescent solar concentrators to produce more energy at a lower cost
- Wrote C++ code to numerically integrate a model of light travelling in a complex optical system
- Designing and running experiments testing optical systems exposed to sunlight
- Processing and reducing large amounts of data into meaningful and presentable results
- Synthesizing and testing the performance and photostability of optical-quality polymer films containing DNA-templated fluorescent silver nanoclusters

Teaching Experience:

Teaching Assistant- Introductory Physics Courses (Summer 2015 & 2016, Fall 2017, Spring 2018)

- Assisting during class, handling student questions, and leading them through the learning process
- Presenting course material and running problem-solving review sessions outside of class

Skills:

C++, Microsoft Excel, Java, Python, LaTeX, SQL, UV-VIS/IR/NMR spectroscopies, measuring solar energy electrical conversion, radiometry, polarimetry, fluorometry, Arduino microcontrollers, chemical synthesis and extraction, thin polymer film deposition, Oscail, PASCO, Logger Pro, numerical analysis

Time management: 20+ credits/semester average while working as both a research and teaching assistant

Publications/Presentations/Grants

First author- "Increasing the Area of a White Scattering Background can Increase the Power Output of a Luminescent Solar Concentrator"- submitted to the journal *Solar Energy* (July 2017)

Presenter- American Physical Society 2018 March Meeting (oral) "Increasing the Area of a White Scattering Background can Increase the Power Output of a Luminescent Solar Concentrator"

Presenter-Penn State Behrend Sigma Xi Undergraduate Research Conference

2017- 1st place poster (Physics, Chemistry & Math) "Increasing the Area of a White Diffusive Background can Increase the Power Output of a Luminescent Solar Concentrator"

2016- 1st place poster (Physics & Chemistry) "Understanding the Effects White Diffusive Backgrounds have on Luminescent Solar Concentrators"

Wrote and awarded 5 Undergraduate Student Research Grants, over $4,000 total (2016-2018)

Academic Awards:

Council of Fellow Undergraduate Research Award (2018)

Academic Excellence in Physics Award (2018)